DE GRUYTER
OPEN
10.1515/tvsb-2016-0020

Transactions of the VŠB – Technical University of Ostrava
Civil Engineering Series,Vol. 16, No. 2, 2016
paper #20

Josef KVĚTOŇ[1], Jan ELIÁŠ[2]

DISCRETE MODEL FOR CONCRETE FRACTURE: NUMERICAL STUDY OF DYNAMIC RESPONSE

Abstract

The contribution presents simulations on concrete specimens. The discrete meso-scale particle model with random geometry based on Voronoi tessellation is used. The model was enhanced with dynamic solver based on implicit Newmark method. Model is tested on cantilever beam loaded by a force at the free end to verify the ability of the model to simulate the dynamic behavior of a simple linear elastic material. Results computed with different time discretization and model settings are compared. The behavior of the model in nonlinear regime is investigated on concrete specimens loaded at different displacement rates. The constitutive law used within this contribution is insensitive to strain rate.

Keywords

Discrete model, dynamic response, Newmark method, inertia, strain rate.

1 INTRODUCTION

The dynamic response of structures is often calculated using time discretization based on the finite difference method. Such discretization scheme can be used for continuous models, as well as for models that represent material by a system of interconnected rigid bodies with a finite size. So called discrete/particle models can be conveniently used for simulating meso-scale behavior of heterogeneous materials [7, 4, 2].

Several other similar models have been presented in literature [5, 6, 9], however all of them are built on explicit time integration scheme. Use of explicit time integration is convenient for events of short duration with high rates like impact loading, blast or wave propagation. In case of longer time intervals in low frequencies (such as structural responses on earthquakes), it is quite computationally demanding, mainly because of the necessity of calculating over a large number of a very short time steps to keep the solution stable. It is well known that the stability of implicit methods does not depend on the length of the time step. The only issue is the accuracy and so it determines the maximum time step length.

The second author has been using static version of the discrete model for a long time. This contribution brings an extension of the complex and robust model into the dynamic regime.

2 DISCRETE MODEL

2.1 Elastic behavior

Individual rigid particles in the discrete model are connected via common facets, the model can be understood as a dense lattice structure. Locations of the nodes are generated randomly, connectivity

[1] Ing. Josef Květoň, Faculty of Civil Engineering, Brno University of Technology, Veveří 331/95, 602 00 Brno, Czech Republic, phone: (+420) 541147131, e-mail: kveton.j@fce.vutbr.cz

[2] Ing. Jan Eliáš, Ph.D., Faculty of Civil Engineering, Brno University of Technology, Veveří 331/95, 602 00 Brno, Czech Republic, phone: (+420) 541147132, e-mail: elias.j@fce.vutbr.cz

is provided by Delaunay triangulation, and shape of the rigid bodies is given by Vornoi tessellation. The material model (in general inelastic) applied at the contact of the facets was developed by Gianluca Cusatis [4] and it was verified to be capable of simulating complex concrete behavior. In this section we focus on its elastic dynamic response only.

Elastic constitutive relations of a single contact are following

$$\sigma_N = E_N \varepsilon_N \tag{1}$$

$$\sigma_{M,L} = E_T \varepsilon_{M,L} \tag{2}$$

where σ and ε are stress and strain, respectively, N is a normal direction and M, L are two remaining tangential directions of an orthonormal basis. Parameter αdetermines ratio between normal and shear stiffness which dictates macroscopic Poison's ratio of the system.

$$E_T = \alpha E_N \tag{3}$$

The meso-scopic normal modulus of elasticity, E_N, is the second elastic parameter of the model. An approximate relation between meso-scopic and macro-scopic elastic parameters yields [4]

$$E_N = \frac{1}{1-\nu} E \tag{4}$$

$$\alpha = \frac{1-4\nu}{1+\nu} \tag{5}$$

Eqs. (4) and (5) postulate limitations of the macro-scopic Poison's ratio, $\nu \in (-1, 0.25)$. ν larger than 0.25 results in negative α, which would give us negative shear stiffness in Eq. (3). If we require ν to be larger than 0.25, we could decouple the strain into its volumetric and deviatoric part, but the ability of the model to represent transversal tension when loading in pressure would be lost. However, since we want to use the model to represent concrete with Poison's ratio about 0.2, the limitation takes no effect.

Nevertheless, Eqs. (4) and (5) are just approximate relations, using these in a material model gives us the macroscopic response a little stiffer than it should be (of a few percent). The more accurate values can be obtained numerically by fitting elastic deformation computed by the discrete model with the equations of the theory of elasticity.

The construction of the model geometry and its elastic behavior is described in detail in [8].

2.1 Nonlinear behavior

Constitutive relations described in previous section apply for model behavior in elastic regime only. Nonlinear behavior is assumed according to [4]. The model was further improved in [5, 6]. It is one of the most robust models for concrete behavior.

The version of the model we use is based on damage mechanics. Each contact between two particles is assigned with damage parameter, $\omega \in \langle 0,1 \rangle$. Equations (1-2) become

$$\sigma_N = (1-\omega) E_N \varepsilon_N \tag{6}$$

$$\sigma_{M,L} = (1-\omega) E_T \varepsilon_{M,L} \tag{7}$$

Evolution of damage parameter is driven by maximum reached equivalent strain. Its description is quite complex and can be found in detail in [4]. All constitutive relations are independent of strain rate.

3 DYNAMICS

The methods for time discretization are divided into the explicit and implicit schemes. Briefly speaking, the explicit one assembles the motion equations at time t in order to estimate structural behavior between times t and $t + \Delta t$, while the implicit one does it at time $t + \Delta t$. The explicit methods are conditionally stable depending on the time step length and the smallest natural frequency. On the other hand, their implementation is relatively easy and suitable for parallelization. Implicit methods

need to assemble mass and stiffness matrices and then solve large system of nonlinear equations. However, thanks their unconditional stability, they can be conveniently used for solution over longer time intervals. We decided to use implicit Newmark method [11]. To get the displacement in time $t + \Delta t$, we are solving the equation

$$\left(\boldsymbol{K} + \frac{1}{\beta \Delta t^2}\boldsymbol{M} + \frac{\gamma}{\beta \Delta t}\boldsymbol{C}\right)\boldsymbol{u}_{t+\Delta t} =$$

$$\boldsymbol{F}_{t+\Delta t} + \boldsymbol{M}\left(\frac{1}{\beta \Delta t^2}\boldsymbol{u}_t + \frac{1}{\beta \Delta t}\dot{\boldsymbol{u}}_t + \left(\frac{1}{2\beta} - 1\right)\ddot{\boldsymbol{u}}_t\right) + \boldsymbol{C}\left(\frac{\gamma}{\beta \Delta t}\boldsymbol{u}_t + \left(\frac{\gamma}{\beta} - 1\right)\dot{\boldsymbol{u}}_t + \frac{\Delta t}{2}\left(\frac{\gamma}{\beta} - 2\right)\ddot{\boldsymbol{u}}_t\right) \quad (8)$$

where $\boldsymbol{K}, \boldsymbol{M}, \boldsymbol{C}$ are stiffness, mass and damping matrices, respectively; $\boldsymbol{F}$ is a loading vector and $\boldsymbol{u}, \dot{\boldsymbol{u}}, \ddot{\boldsymbol{u}}$ are displacement, velocity and acceleration vectors, respectively, β and γ are constants of the Newmark method [11]. The velocity and acceleration at time $t + \Delta t$ are calculated from displacements

$$\ddot{\boldsymbol{u}}_{t+\Delta t} = \frac{1}{\beta \Delta t^2}(\boldsymbol{u}_{t+\Delta t} - \boldsymbol{u}_t) - \frac{1}{\beta \Delta t}\dot{\boldsymbol{u}}_t - \left(\frac{1}{2\beta} - 1\right)\ddot{\boldsymbol{u}}_t \quad (9)$$

$$\dot{\boldsymbol{u}}_{t+\Delta t} = \dot{\boldsymbol{u}}_t + \Delta t(1-\gamma)\ddot{\boldsymbol{u}}_t + \gamma \Delta t \ddot{\boldsymbol{u}}_{t+\Delta t} \quad (10)$$

To make the method implicit and thus the solution unconditionally stable, we have to keep Newmark constants in the following limits

$$2\beta \geq \gamma \geq 0.5 \quad (11)$$

When $\beta = 0.25$ and $\gamma = 0.5$, the method is using trapezoidal rule for integration in time and it lies at the border between implicit and explicit regimes.

The damping matrix included in Eq.(8) influences mainly elastic behavior, however, for the purpose of this contribution, it is neglected. When nonlinear material behavior is applied, the model is damped by dissipation of energy at the contact facets.

3.1 Mass matrix

Lumped mass matrix is commonly used in dynamic simulations. Such simplification neglects the influence of the moments of inertia and takes into account only the mass of particle concentrated in its center. However, neglecting the inertia moments might provide inaccurate solution. Here, we consider the influence of the moments of inertia and the mass matrix is not diagonal.

The rigid bodies obtained from Voronoi tessellation are convex polyhedrons. To calculate the inertia moments, these polyhedrons are decomposed into simplexes (tetrahedrons) for which analytical formula for inertia tensor exists [13]. These tensors are combined using the Steiner's (parallel axis) theorem.

Since the mass matrix is based on the geometry of rigid particles and the fracture is allowed only on their contacts, the matrix itself is considered constant over the whole solution time.

4 NUMERICAL EXAMPLES

4.1 Elastic cantilever beam

The elastic behavior of the model is tested using a cantilever beam loaded by a force F = 1 N at the free end (Fig. 1). Its dimensions are following: length L is 200 mm, depth and width are 20 mm. Particle radii, parameters of the Newmark method and the time step length are varying In order to investigate the influence of their change on the model behavior. For comparison, one (reference)

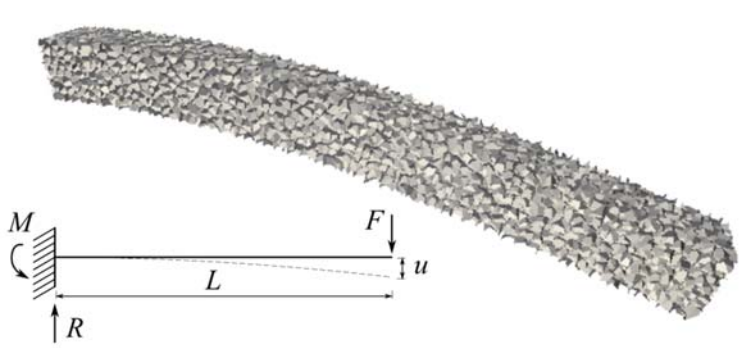

Fig. 1 Settings of the cantilever beam and deformed shape showing the model structure (deformation magnified 250 times).

setting is kept in all studies the same: particle radius 2 mm, time step 0.05 ms and parameters $\beta = 0.25$ and $\gamma = 0.5$. We should also mention that the material is considered as linearly elastic and damping matrix is neglected.

Simplifying the cantilever as an ideal beam and assuming that it is vibrating in its first natural shape only, the deflection of the free end can be calculated analytically. The solution is

$$u(t) = cos(\omega_I t)\frac{FL^3}{3EI} - \frac{FL^3}{3EI} \tag{12}$$

where F stands for loading force at the free end, L for length of beam, E is elastic modulus and I is moment of inertia of beam cross section. The first natural frequency ω_I can be expressed

$$\omega_I = \lambda_I \sqrt{\frac{EI}{mL^3}} \tag{13}$$

where λ_I is according to [3] equal to 1.875. In all the graphs in following subsections, this analytical solution is plotted in gray while static solution appears as thin straight line.

The response of the model is shown as two graphs in Fig. 2-4. Each time, the upper graph displays evolution of deflection u of the free end in time, and the lower one the time dependence of the vertical reaction R in the support. Every figure shows the sensitivity of the model to the change of one input parameter.

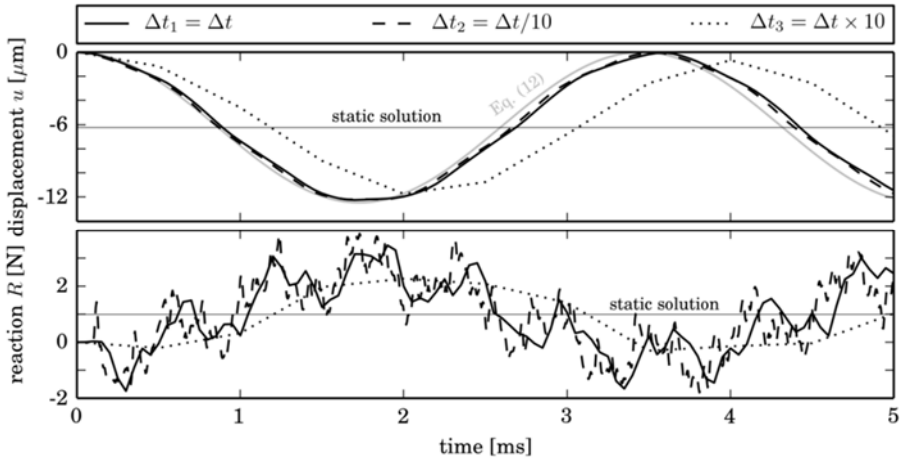

Fig. 2 Dynamic response of cantilever beam using various time discretization.

At first we examined the solution with different length of the time step. Graphs in Fig. 2 show the response of cantilever beam loaded by constant force $F = 1\text{N}$. Time step length is Δt =0.05 ms and 10 times shorter and longer, respectively. On the lower graph, we can observe that the longer the time step, the more high frequencies are damped as a side effect of numerical solution. The difference between two finer time discretizations is quite small compared to the difference between any of them and longest time step. Greater oscillations are caused by the fact that for the shorter time step length, the initial "impact" of the constant force happens in shorter time.

For damping of high order modes it is recommended to use Newmark constants not only within limits according to Eq. (9), but to satisfy also [1]

$$\beta \geq 0.25(0.5 + \gamma)^2 \tag{14}$$

Fig. 3 shows the dependence of the model behavior on change of the parameters of the Newmark method, beam is loaded by the same constant force. It can be seen, that if we use the parameters for the trapezoidal rule ($\beta = 0.25$ and $\gamma = 0.5$), we are taking into account more high order modes than if we use large values of these parameters. The response then becomes smoother.

Since the model is based on a concept of rigid body motion of particles of finite size, it is important to know the influence of their size. In all simulations, particle size is 2 mm, which gives us

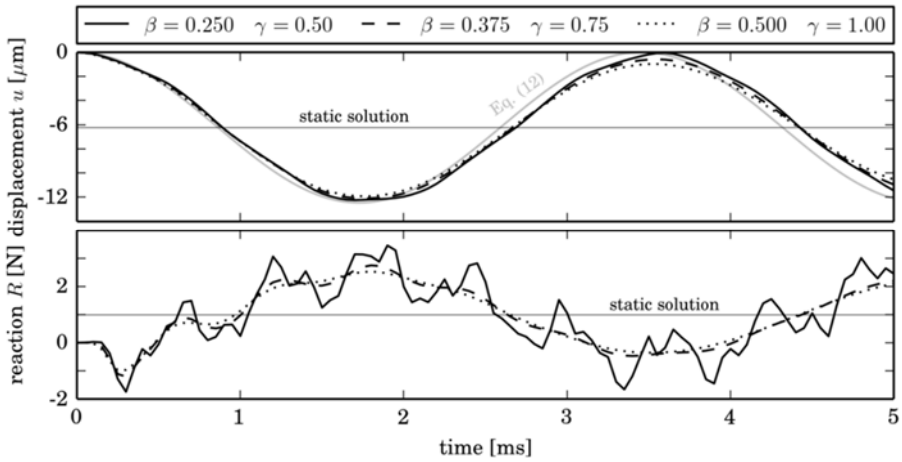

Fig. 3 Dynamic response of cantilever beam using various parameters of Newmark method

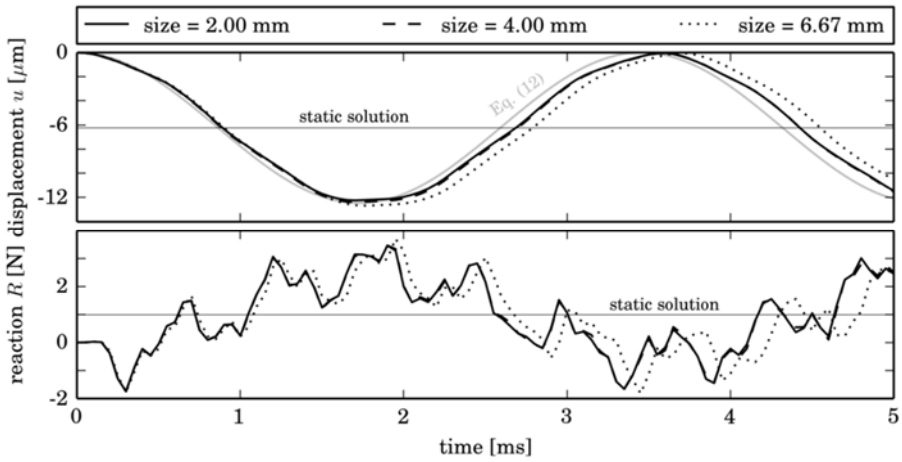

Fig. 4 Dynamic response of a cantilever beam using different particle size.

approximately 10 bodies per cross section depth/width. In Fig. 4, the change of response with change of the body size is shown. The difference is obvious particularly for size 6.67 mm. In this case, only 3 particles are filling the depth/width of the beam.

4.2 L-shape concrete specimen

So far we have been discussing elastic behavior of the model, but our ambition is to simulate real concrete behavior. To demonstrate the nonlinear material behavior of the model, we chose the geometry used by Ožbolt in [12]. The article provides data from experimental series as well as numerical simulations using FEM. It documents excellent match between experimental and numerical responses.

It is well known that the loading capacity is dependent on the strain rate. In case of quasi-static loading, the initial micro cracks localize into one highly damaged zone. With increasing strain rate the amount of energy dissipated in specimen body increases and the crack branches [10]. At the end, the damaged zone is larger, but it also consumes more energy. Damaging specimens under higher strain rate typically leads to increase of the loading forces. For the higher loading rates, the progressive increase of loading force is controlled mostly by inertia effects and not by the rate dependent strength of concrete [12]. Motivated by that, we would like to keep the constitutive law strain-rate independent.

The simulated specimen is shaped as upside-down letter L, its depth D_0 and width W are 500 mm and thickness is 50 mm. Depth D_1 is 250 mm, setting of specimen is shown in Fig. 5 left. The loading force F shown in the figure is measured during the simulation, but the loading is applied by deformation.

Material parameters considered according to [4] are following: tensile strength f_t = 3.12 MPa, compressive strength f_c = 46.25 MPa and material density 2210 kg/m3. The elastic properties were converted to correspond to the meso-scale parameters of the model (Eq. 4-5) and the used values are: modulus of elasticity EN = 40 GPa, parameter α = 0.24.

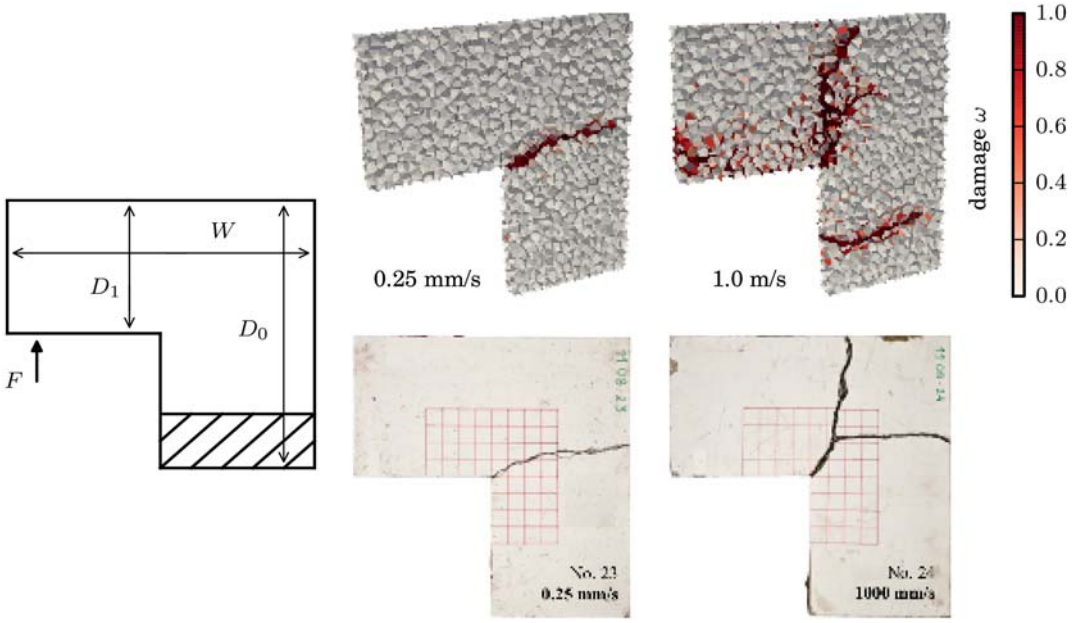

Fig. 5 Specimen settings (left) and different crack pattern for different strain rates obtained by the particle model (upper) and experimentally [12] obtained crack pattern (lower)

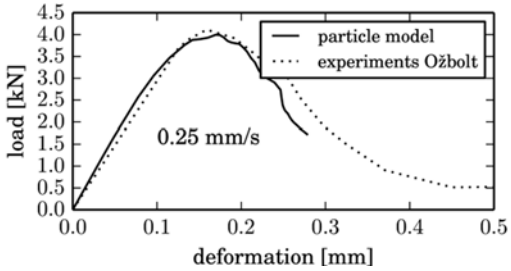

Fig. 6 Load – displacement response for the quasi-static loading

The specimen response was calculated for the case of quasi-static loading (displacement rate 0.25 mm/s) and further for displacement rate 1.0 m/s. The value of meso-scale tensile fracture energy was obtained from fitting the maximum load of the experimental response [4] for quasi-static loading. Obtained value is $G_f = 35.5$ N/m. The load – displacement responses of both model and the experiment are shown in Fig. 6.

For the quasi-static loading, the crack direction is horizontal (Fig. 5 center). When increasing loading velocity, the angle of crack direction from horizontal line tends to increase. When we increase the rate further, the energy accumulated in specimen body exceeds the amount that can be dissipated in just one crack and more crack branches appear. This trend of crack inclination and branching can be observed in the right part of Fig. 5. For loading rate 1.0 m/s the main crack initiates from the specimens corner and splits into two crack branches. This is in agreement with experimental crack pattern (Fig. 5). In the later stages of simulation new cracks also appear in the area of applied load and close to the support. Fig. 7 shows evolution of the loading force in time for displacement rate 1.0 m/s. Though there is substantial increase in peak load compared to quasi-static loading, it is not sufficient to match the experiments.

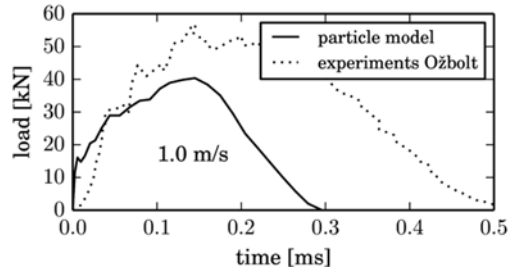

Fig. 7 Load – time response for loading under the displacement rate 1.0 m/s

5 CONCLUSION

The discrete model for concrete fracture has been extended by an implicit dynamic solver. The functionality of this enhancement was presented in a simple study of the time dependent response of an elastic cantilever beam. The sensitivity of the model to change of input parameters was shown. The time dependent behavior was investigated also in nonlinear regime. Two simulations were calculated to show the ability of the model to predict different concrete behavior at different strain rates. The results correspond to the experiments. The strain rate effect should automatically arise from the inertia, constitutive law is independent of the strain rate. The results show substantial but insufficient increase of loading force when compared to the experiment.

It is true that damping could further increase the load, but paper [12] shows good correspondence of the model and experiments even without any damping. The discrepancy may also be caused by cracking in the loading and supporting area. Such a cracking is not reported in [12]. However, the cracks are present in all the model versions we tested. Up to now, the reason why the

loading force does not reach the experimentally measured value is not found. The authors will continue in the effort to resolve this issue.

ACKNOWLEDGEMENT

The financial support provided by the Ministry of Education, Youth and Sports of the Czech Republic under the project LO1408 ‘‘AdMaS UP - advanced Materials, Structures and Technologies’’ under ‘‘National Sustainability Programme I’’ is gratefully acknowledged.

LITERATURE

[1] BATHE, K-J. *Finite element procedures*. Englewood Cliffs, N.J.: Prentice Hall, 1996. ISBN 01-330-1458-4.

[2] BOLANDER, J.E. a S. SAITO. Fracture analyses using spring networks with random geometry. *Engineering Fracture Mechanics*. 1998, 61(5-6), 569-591. DOI: 10.1016/S0013-7944(98)00069-1. ISSN 00137944

[3] BREPTA, R., PŮST, L., TUREK, F.: *Mechanické kmitání*, Technický průvodce 71, nakladatelství Sobotáles, Praha, 1994

[4] CUSATIS, G., CEDOLIN, L., Two-scale study of concrete fracturing behavior, Engineering Fracture Mechanics, 74(12): 3–17, 2007, ISSN 0013-7944.

[5] CUSATIS, G., PELESSONE, D. Mesolevel simulation of reinforced concrete under impact loadings. In *Computational Modelling of Concrete Structures - Proceedings of EURO-C 2006*, pages 63–70, Mayrhofen, Austria, 2006. EURO-C 2006 Conference.

[6] CUSATIS, G., BAŽANT, Z. P., CEDOLIN, L. Confinement-shear lattice model for concrete damage in tension and compression. *Journal of Engineering Mechanics*, vol. 129(12):1439{1448, 2003. ISSN 0733-9399. doi: 10.1061/(ASCE)0733-9399(2003)129:12(1439).

[7] ELIÁŠ, J., VOŘECHOVSKÝ, M., SKOČEK, J., BAŽANT, Z-P. Stochastic discrete meso-scale simulations of concrete fracture: comparison to experimental data. *Engineering Fracture Mechanics* 135, pp. 1-16, 2015, ISSN: 0013-7944, doi: 10.1016/j.engfracmech.2015.01.00

[8] ELIÁŠ, J., Adaptive refinement technique for discrete static models of fracture. In: Proceedings of Particle-based Methods IV – Fundamentals and Applications, Barcelona, Spain, September 28-30, 2015. E. Oñate, M. Bischoff, D.R.J. Owen, P. Wriggers and T. Zohdi (Eds.). International Center for Numerical Methods in Engineering (CIMNE), pp. 320–332. ISBN 978-84-944244-7-2.

[9] FRANTÍK, P.; VESELÝ, V. Simulation of the fracture process in quasi- brittle materials using a spring network model. In *Proceedings of 17th International Conference Engineering mechanics 2011*. Svratka: 2011. s. 147-150. ISBN: 978-80-87012-33- 8.

[10] JIRÁSEK, M., BAŽANT, Z.P. Particle model for quassibrittle fracture and application to sea ice. *J. Eng. Mech.*,121(9):1016-1025, 1995. doi: 10.1061/(asce)0733-9399(1995)121:9(1016)

[11] NEWMARK, N. *A method of computation for structural dynamics*. Urbana: University of Illinois, 1959.

[12] OŽBOLT, J., BEDE, N., SHARMA, A., MAYER, U.. Dynamic fracture of concrete L-specimen: Experimental and numerical study. Engineering Fracture Mechanics. 2015, 148, 27-41. doi: 10.1016/j.engfracmech.2015.09.002.

[13] TONON, F. Explicit exact formulas for the 3-d tetrahedron inertia tensor in terms of its vertex coordinates. *Journal of Mathematics and Statistics*, vol. 1(1):8–11, 2005-1-1. ISSN 15493644. doi: 10.3844/jmssp.2005.8.11.